Applied Physics Letters

# Twisted pillared phononic crystal plates

Cite as: Appl. Phys. Lett. **120**, 232202 (2022); https://doi.org/10.1063/5.0097082
Submitted: 25 April 2022 • Accepted: 26 May 2022 • Published Online: 10 June 2022

Mourad Oudich, Yuanchen Deng and Yun Jing



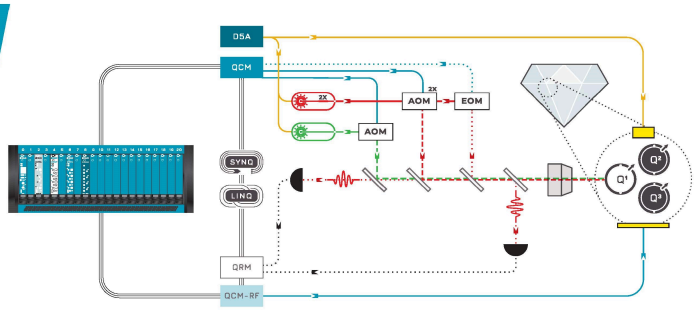

Applied Physics Letters ARTICLE scitation.org/journal/apl

# Twisted pillared phononic crystal plates

Cite as: Appl. Phys. Lett. **120**, 232202 (2022); doi: 10.1063/5.0097082
Submitted: 25 April 2022 · Accepted: 26 May 2022 ·
Published Online: 10 June 2022



Mourad Oudich,[1,2,a)] Yuanchen Deng,[1] and Yun Jing[1,a)]

## AFFILIATIONS

[1]Graduate Program in Acoustics, The Pennsylvania State University, University Park, Pennsylvania 16802, USA
[2]Université de Lorraine, CNRS, Institut Jean Lamour, F-54000 Nancy, France

**Note:** This paper is part of the APL Special Collection on Acoustic and Elastic Metamaterials and Metasurfaces.
[a)]**Authors to whom correspondence should be addressed:** mourad.oudich@univ-lorraine.fr and yqj5201@psu.edu

## ABSTRACT

Recent discoveries in twisted heterostructure materials have opened research directions in classical wave systems. This Letter investigates a family of double-sided pillared phononic crystal plates as the elastodynamic analog of bilayer graphene, including twisted bilayer graphene. The phononic crystal plate design is first validated by studying the basic AA- and AB-stack configurations under weak interlayer coupling. A specific commensurate twist angle giving rise to the sublattice exchange even symmetry is then studied to examine the twist-modulated band structure. Finally, this study demonstrates that the same twist angle, in concert with an ultra-strong interlayer coupling, can collectively create valley-dependent edge states that have not been previously observed in electronic bilayer graphene.



The field of twisted heterostructures, also known as twistronics, has enriched the physics and expanded the family of two-dimensional materials.[1] One type of twisted heterostructure of particular interest is twisted bilayer graphene (TBG), which has been extensively studied for its electronic band modulated by the twist degree of freedom.[2–4] Twisting two layers of graphene creates the so-called Moiré pattern, which can radically alter the electronic,[2–4] optical,[5] and thermal[6] properties of bilayer graphene. It was discovered that at some discrete twist angles (the so-called magic angles), the smallest being around 1.08°, the electronic band structure of TBG displays flat bands at the zero energy level,[2] which can be harnessed for unconventional superconductivity and correlated Mott insulating states.[3,4] Furthermore, some large twist angles can also lead to flat bands due to geometric frustration[7] or render the TBG a higher-order topological insulator.[8]

Meanwhile, there has been a strong interest in using mechanical wave systems as a versatile platform for mimicking condensed matter phenomena. Specifically, quantum-like mechanical phenomena have been demonstrated at the mesoscopic and macroscopic scales using phononic crystals (PCs). This has enabled unprecedented acoustic and elastic wave control, such as topological interface, edge and corner states,[9–13] Weyl points,[14–17] and topological pumping.[18–20] It then becomes natural to also explore the equivalent mechanical design of TBG to investigate quantum-inspired devices. Multiple studies have recently attempted to pursue this direction under the framework of acoustics[21–25] and elastodynamics,[26–28] to analyze the dispersion of the classical AA and AB stacking configurations,[21–23,26,28] to demonstrate the existence of flat bands at the magic angles,[23,24] or to evidence twist-dependent resonance states.[27] In the context of elastodynamics, for example, Rosendo López *et al.*[26] considered two weakly coupled plates with interacting flexural waves, where each plate is decorated with a hexagonal lattice of pillar resonators, and demonstrated the emergence of elastic flat bands at the magic angles. In contrast, Martí-Sabaté and Torrent[27] considered a cluster of scatterers distributed in a Moiré pattern over a thin elastic plate. They showed the existence of localized dipolar resonances at a series of discrete "twist" angles. Jin *et al.*[28] introduced the design of a thin plate where both sides are decorated with a hexagonal lattice of pillars. They adopted an AA stacking configuration (top and bottom pillars are aligned) to study the topology of the bands and demonstrated enhanced Valley state transport. The robustness of the edge state against angle misalignment was also studied. Yves *et al.*[29] designed an elastic metasurface made of a lattice of pillars with spatially modulated heights in a Moiré pattern, to enable topological transition of the isofrequency contour from hyperbolic to elliptical dispersion. Pillared phononic crystal plates have proven to be an effective platform for efficient elastic wave manipulation.[30]

This paper presents a double-sided PC plate, or a bilayer PC (BPC), where the band structures of AA-stacking, AB-stacking, and twisted bilayer with even sublattice exchange (SE) symmetry exhibit band dispersions mirroring those of the classical TBG under weak interlayer coupling. Previous works have not investigated these analogs between bilayer graphene and elastic PCs. In addition, this work also shows valley Hall edge states as a result of the interplay between twist

degree of freedom and ultra-strong interlayer coupling. Specifically, it is discovered that twisted BPC (TBPC), under ultra-strong interlayer coupling, can display a well-isolated low-frequency Dirac cone for flexural waves, which is unattainable by its monolayer counterpart. This Dirac cone can be leveraged to induce valley Hall edge states by breaking the symmetry of the lattice. While the BPC design studied in this work is similar to the one reported by Jin *et al.*,[28] it is noted that these two works are still fundamentally different. For example, only strong interlayer coupling was studied in Jin *et al.*[28] Additionally, while the twist was treated as a defect by Jin *et al.*[28] for studying the robustness of bilayer valley Hall edge states, the present work harnesses twist as an essential ingredient for valley Hall edge states.

First, a hexagonal (graphene-like) lattice of identical pillars distributed over the surface of a semi-infinite substrate is considered, which supports the propagation of surface acoustic wave (SAW) [see Fig. S1(a) in the supplementary material). The structure is made of aluminum where the distance between the closest pillars is $a = 10$ mm (lattice constant $a_0 = a\sqrt{3}$), and the radius and height of the pillars are $r = 3.7$ mm and $L = 12$ mm, respectively. Using COMSOL Multiphysics 5.4, the numerically calculated band structure for SAW is shown in Fig. S1(b) (supplementary material). The elastic modes that have dominant vibration along the axis of the cylindrical pillars, namely, the $z$ direction, are the focus of this study. To this end, the polarization of the modes is characterized by calculating the amplitude weight of the displacement field component along the $z$ direction using the following equation:

$$\hat{u}_z = \int \frac{|u_z|^2}{|u_x|^2 + |u_y|^2 + |u_z|^2} dv, \tag{1}$$

where the integral is taken over the considered volume of the substrate and $u_x$, $u_y$, and $u_z$ are the three components of the displacement vector.

In the band structure plot, the modes with dominant $u_z$ component are highlighted by adopting a gray to red color scale. Bands in gray color are for $\hat{u}_z$ that are close to zero (gray), which are associated with mainly in-plane polarization, while this parameter becomes closer to 1 (red) when the mode is mainly polarized along the out-of-plane direction $z$. From Fig. S1(b), the dispersion of SAW displays a Dirac cone at 77.7 kHz under the sound line. Both modes at the degeneracy are associated with vertical resonances of the pillars.

Afterward, the bilayer configuration is constructed by considering a plate where both surfaces can support Rayleigh waves. Now consider a double-sided hexagonal lattice of pillars [Fig. 1(a)], it can be expected that the elastic surface modes would couple between the two layers via evanescent waves. This coupling is consequently the analog of the interlayer hopping in classical bilayer graphene. The choice of the thickness of the plate dictates the strength of this coupling in our BPC design. If the plate's thickness is sufficiently larger than twice the penetration depth of the Rayleigh waves, the mode's coupling between the two surfaces can be considered weak.

First the elastic wave dispersion for the AA and AB stacking BPC under weak interlayer coupling is investigated. The unit cells are shown in Figs. 1(b) and 1(c) for a plate thickness of 25 mm. The dispersion curves are displayed around the Dirac cone's frequency where one can observe that the band structure of AA stacking displays two crossing bands at the $K$ point [Fig. 1(b)], while that of AB stacking configuration shows a quadratic dispersion with a degeneracy at the $K$ point [Fig. 1(c)]. These behaviors bear strong similarities to those of the classical AA and AB stacking bilayer graphene.[31] The full band

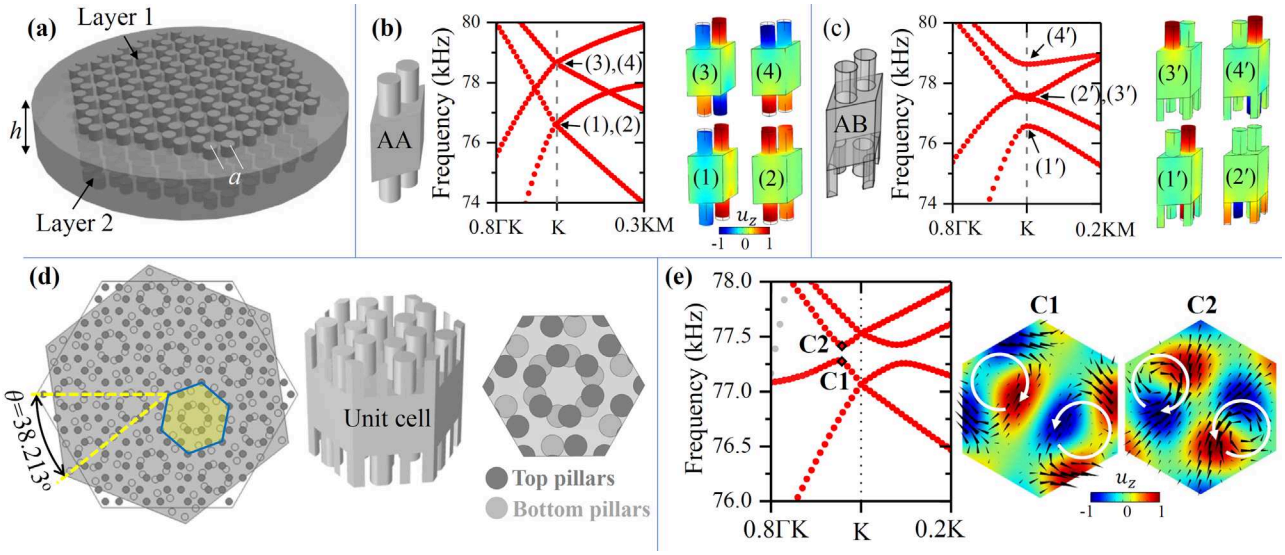


**FIG. 1.** (a) The bilayer PC constructed by decorating both surfaces of a plate by two hexagonal lattices of pillars. The band structures of AA (b) and AB (c) stackings along with the associated unit cells and the displacement field component $u_z$ for four bands at the $K$ point. (d) A TBPC at the commensurate angle of 38.213°, which gives a periodic lattice with an even sublattice exchange symmetry. (Left to right) The TBPC with the unit cell highlighted by the shaded yellow region; 3D view of the unit cell; planar schematic of the unit cell where the positions of the top and bottom pillars are highlighted in the dark and light gray colors, respectively. (e) The band structure around the Dirac frequency, close to the $K$ point, showing a narrow bandgap. The figure on the right shows the wavefield component $u_z$ in the unit cell at points C1 and C2 marked in the band structure. The black conical arrows indicate the Poynting vector, and the white circular arrows are added for a better visualization of the directional energy flux.

structures for these stacking configurations are presented in the supplementary material. Furthermore, to understand the dynamical behavior of our system, the vibrational motion of the bilayer at the $K$ point is analyzed by plotting the displacement component $u_z$ for the unit cell [Figs. 1(b) and 1(c)]. For both stacking configurations, it is observed that the modes are associated with the vertical resonance of the pillars on both layers. For the case of AA stacking, the two lower modes indicated by (1) and (2) in Fig. 1(b) display pillar vibration with an asymmetric motion with respect to the middle plane of the plate, while the two pillars of each layer are out-of-phase in the case of mode (1) and in-phase for mode (2). However, an opposite behavior is observed in the two upper modes denoted (3) and (4), where the dynamic motion of the pillars is symmetric with respect to the middle plane of the plate while the two pillars in the same layer have out-of-phase vibration in the case of mode (3) and in-phase motion for mode (4). These four modes display the four possible in-phase and out-of-phase vibrational motions of the four pillars in the unit cell. In the case of AB stacking [Fig. 1(c)], a close look into the vibrational motion of the pillars reveals that the lower and upper modes indicated respectively by (1′) and (4′) in the band structure are only associated with the resonance of the pillars that are facing each other from the two layers. In addition, in the lower mode (1′), the two pillars facing each other have an asymmetric vibrational motion with respect to the middle plane of the plate while the vibration of mode (4′) is symmetric. The touching bands at point $K$ [modes indicated by (2′) and (3′)] are associated with the resonance of the pillars in only one layer and only for the pillars that face the center of the hexagon of the other layer.

BPC with a twist is then investigated. Twisting creates the Moiré pattern, which is in general quasiperiodic, but becomes perfectly periodic for discrete values of the twist angles, known as commensurate angles.[32] The commensurate angle of 38.213° is chosen, which gives a lattice with an even sublattice exchange symmetry.[33] Figure 1(d) displays the twisted bilayer structure at 38.213°. For the sake of clarity, a planar representation of the unit cell is shown, where the dark and light gray disks correspond to upper and bottom layers, respectively. The six corners of the hexagonal cell have pillars from both layers facing each other [see 3D representation of the unit cell in Fig. 1(d)]. This unit cell has a $C_6$ symmetry. The band structure is computed and shown in Fig. 1(e) around the Dirac cone frequency for the plate thickness of 22.5 mm, which again corresponds to a weak interlayer coupling. One can observe that the dispersion, within the wave-vector range shown here, displays a narrow bandgap from 77.28 to 77.42 kHz. This band structure near the $K$ point is similar to what was shown for the twist bilayer graphene at the same angle.[33] It should also be noted that this bandgap only exists for a certain range of weak interlayer coupling. For example, the bandgap closes at the plate thickness of 25 mm. The eigenmodes for the unit cell at the edges of this bandgap [points C1 and C2 in the band structure of Fig. 1(e)] are also plotted, and it is discovered that the gap is associated with the pseudospin behavior[33,34] characterized by rotational out-of-plane displacement field that is highlighted by evaluating the elastic Poynting vector [black conic arrows in the wave fields in Fig. 1(e)]. White circular arrows are also added for a better visualization of the directional energy flux. Note that this specific bandgap has been previously shown to host topological corner modes.[8,34]

We further our study by investigating the effect of increasing the interlayer coupling between the surface modes through significantly reducing the thickness of the plate from 22.5 to 3 mm [Fig. 2(a)]. It is noted that at this thickness, the propagating elastic wave should be considered as flexural wave. The band structure [the middle figure of Fig. 2(b)] of this lattice displays a Dirac cone that appears at a very low frequency, i.e., 39.5 kHz. Here, the radius of the pillar is adjusted to 3 mm (reduced from 3.7 mm) to have a well-isolated Dirac cone and more importantly to avoid cutting the pillars inside the unit cell when constructing the topological interface which will be explained later. Other parameters of the pillars are kept the same. Under this pillars size, the monolayer Dirac cone lies at 80.2 kHz, which is twice as high. The interlayer coupling, thus, can be leveraged as an effective tool to engineer the elastic wave dispersion of BPC.

Due to the $C_6$ symmetry with a single Dirac degeneracy at the $K$ point, we explore the possibility of creating valley Hall edge states by reducing $C_6$ symmetry to $C_3$ symmetry. To do so in the unit cell, two sets of pillars distribution are considered: the first set, indicated in purple and pink colors in Fig. 2(c), will undergo a counterclockwise rotation of $\varphi$, while the second set, shown in light and dark gray, will be rotated by $\varphi$ clockwise with respect to the center of the unit cell. This symmetry reduction lifts the degeneracy and opens a bandgap, which is indicated by yellow and orange shaded regions in Fig. 2(b) for the cases of $\varphi = 3°$ and $\varphi = -3°$, respectively. To gain more insights about the physical behavior of the modes at the valley, Fig. 2(d) displays the evolution of the two valley states as function of the rotation angle $\varphi$, and the out of plane components amplitude $|u_z|$ and its phase distribution in the unit cell for the upper and lower edges of the bandgap at the $K$ point for $\varphi = 3°$ and $\varphi = -3°$. From the phase distribution, the out-of-plane modes can be viewed as propagating pseudospin modes where the upper and lower valley modes for $\varphi < 0$ have clockwise and anticlockwise pseudospins, respectively, and inversely for $\varphi > 0$. A mode inversion can be observed when comparing the modes shown on the left and right. The bandgap is marked by different colors (yellow or orange) depending on its different topological characteristics. It is expected that propagating valley topological edge modes will emerge in the presence of an interface with different signs of $\varphi$. A zigzag interface [shown in Fig. 3(a)] is constructed by considering a super cell made of unit cells with $\varphi = 3°$ and $= -3°$. Its band structure is computed with the focus on flexural modes, which are distinguished using Eq. (1). Figure 3(b) shows the valley interface state inside the bandgap with negative group velocity. The right panel shows the displacement field component $u_z$ in the supercell, indicated by the circled state in the band structure. The confinement of the mode at the zigzag interface is evident. To highlight the edge state's backscattering immunity, a waveguiding interface between the two topologically distinct lattices of $\varphi = 3°$ and $\varphi = -3°$ is created with two sharp bendings of 120° [Fig. 3(c)]. To excite the edge state, we applied an out-of-plane (vertical) boundary load on the top surface of a pillar located very close to the interface (indicated by a cyan star in the figure). The displacement field shows that the propagation of wave is robust against the defects introduced by the bendings.

In conclusion, this work studies a family of double-sided pillared phononic crystal plate with hexagonal lattices under both weak and strong interlayer coupling. When a weak interlayer coupling is involved, this elastic wave material behaves similarly to the classical bilayer graphene, and this is confirmed by studying the band structures of AA- and AB-stacking configurations as well as the SE even symmetry resulted from a large twist angle at 38.213°. An advantage of the proposed TBPC compared with the classical TBG is that the

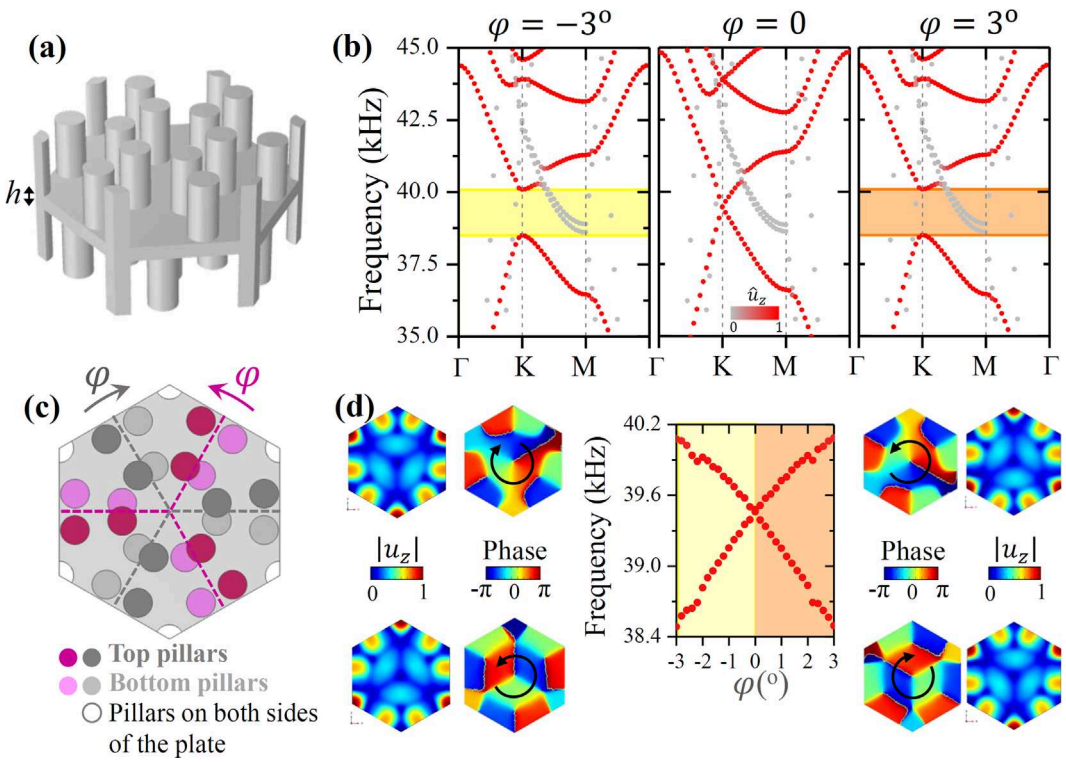


**FIG. 2.** (a) Unit cell of the SE even lattice where the plate thickness is $h = 3$ mm. (b) Band structures of the TBPC for different rotational angles $\varphi = -3°$, $\varphi = 0°$, and $\varphi = 3°$ indicated in (c). (c) Schematic view of the unit cell where the dark and light colors (either gray or purple) indicate the positions of top and bottom pillars, respectively. White pillars at the corners indicate pillars on both sides of the plate, which are aligned in this case. To break the $C_6$ symmetry, we rotate the set of gray pillars by $\varphi$ clockwise and the set of purple and pink pillars by the same angle counterclockwise. (d) Frequency evolution of the two valley states as function of the rotation angle $\varphi$, and the out of plane component amplitude $|u_z|$ and its phase distribution in the unit cell for the upper and lower edges of the bandgap at the *K* point for $\varphi = 3°$ and $\varphi = -3°$.

interlayer coupling strength can be readily manipulated through changing the thickness of the plate. This study shows that, by introducing an ultra-strong interlayer coupling, a low-frequency Dirac cone can emerge for the SE even symmetric TBPC. This Dirac cone can be further utilized to introduce the valley Hall effect for robust wave propagation. Our work provides a fresh perspective on the design of elastodynamic PC, which can potentially benefit applications, such as energy harvesting and NDE.

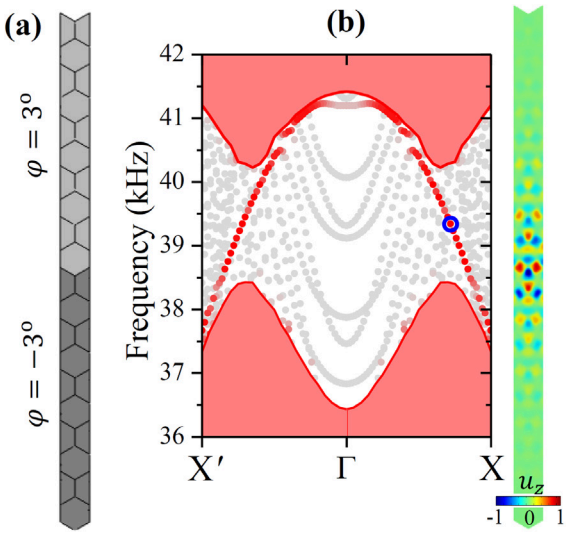


**FIG. 3.** (a) A supercell with an interface constructed from lattices with different band topologies with $\varphi = 3°$ and $\varphi = -3°$. (b) Band structure calculated for the super-cell with the flexural edge state of the plate distinguished with red color, while the modes with gray color being in-plane modes. The shaded light red areas correspond to bulk flexural modes. The side figure shows the displacement field component $u_z$ of the plate at the point indicated by the blue circle on the edge state band. (c) Robust elastic wave propagation in a waveguide with bending constructed by the two topological distinct lattices with $\varphi = 3°$ and $\varphi = -3°$.

See the supplementary material for the full band structures for the pillared phononic surface, the bilayer phononic crystals with AA and AB stacking configurations, and the twisted bilayer with SE even.

The authors would like to thank NSF for the support through No. CMMI-2039463.

## AUTHOR DECLARATIONS

### Conflict of Interest

The authors have no conflicts to disclose.

### Author Contributions

**Mourad Oudich:** Conceptualization (equal); Data curation (equal); Formal analysis (equal); Investigation (equal); methodology (equal); project administration (equal); software (equal); validation (equal); Visualization (equal); Writing – original draft (equal); writing – review and editing (equal). **Yuanchen Deng:** Writing – original draft (supporting). **Yun Jing:** Funding acquisition (lead); project administration (lead); resources (lead); writing – review and editing (lead).

## DATA AVAILABILITY

The data that support the findings of this study are available from the corresponding authors upon reasonable request.

## REFERENCES

[1]S. Carr, D. Massatt, S. Fang, P. Cazeaux, M. Luskin, and E. Kaxiras, Phys. Rev. B **95**, 075420 (2017).
[2]R. Bistritzer and A. H. MacDonald, Proc. Natl. Acad. Sci. U. S. A. **108**, 12233 (2011).
[3]Y. Cao, V. Fatemi, S. Fang, K. Watanabe, T. Taniguchi, E. Kaxiras, and P. Jarillo-Herrero, Nature **556**, 43 (2018).
[4]Y. Cao, V. Fatemi, A. Demir, S. Fang, S. L. Tomarken, J. Y. Luo, J. D. Sanchez-Yamagishi, K. Watanabe, T. Taniguchi, E. Kaxiras, R. C. Ashoori, and P. Jarillo-Herrero, Nature **556**, 80 (2018).
[5]P. Moon and M. Koshino, Phys. Rev. B **87**, 205404 (2013).
[6]H. Li, H. Ying, X. Chen, D. L. Nika, A. I. Cocemasov, W. Cai, A. A. Balandin, and S. Chen, Nanoscale **6**, 13402 (2014).
[7]H. K. Pal, S. Spitz, and M. Kindermann, Phys. Rev. Lett. **123**, 186402 (2019).
[8]M. J. Park, Y. Kim, G. Y. Cho, and S. Lee, Phys. Rev. Lett. **123**, 216803 (2019).
[9]P. Wang, L. Lu, and K. Bertoldi, Phys. Rev. Lett. **115**, 104302 (2015).
[10]L. M. Nash, D. Kleckner, A. Read, V. Vitelli, A. M. Turner, and W. T. M. Irvine, Proc. Natl. Acad. Sci. U. S. A. **112**, 14495 (2015).
[11]Z. Yang, F. Gao, X. Shi, X. Lin, Z. Gao, Y. Chong, and B. Zhang, Phys. Rev. Lett. **114**, 114301 (2015).
[12]H. Xue, Y. Yang, F. Gao, Y. Chong, and B. Zhang, Nat. Mater. **18**, 108 (2019).
[13]H. Fan, B. Xia, L. Tong, S. Zheng, and D. Yu, Phys. Rev. Lett. **122**, 204301 (2019).
[14]M. Xiao, W.-J. Chen, W.-Y. He, and C. T. Chan, Nat. Phys. **11**, 920 (2015).
[15]F. Li, X. Huang, J. Lu, J. Ma, and Z. Liu, Nat. Phys. **14**, 30 (2018).
[16]B. Xie, H. Liu, H. Cheng, Z. Liu, S. Chen, and J. Tian, Phys. Rev. Lett. **122**, 104302 (2019).
[17]X. Shi, R. Chaunsali, F. Li, and J. Yang, Phys. Rev. Appl. **12**, 024058 (2019).
[18]Z. Chen, Z. Chen, Z. Li, B. Liang, G. Ma, Y. Lu, and J. Cheng, New J. Phys. **24**, 013004 (2022).
[19]M. I. N. Rosa, R. K. Pal, J. R. F. Arruda, and M. Ruzzene, Phys. Rev. Lett. **123**, 034301 (2019).
[20]E. Riva, M. I. N. Rosa, and M. Ruzzene, Phys. Rev. B **101**, 094307 (2020).
[21]J. Lu, C. Qiu, W. Deng, X. Huang, F. Li, F. Zhang, S. Chen, and Z. Liu, Phys. Rev. Lett. **120**, 116802 (2018).
[22]W. Dorrell, H. Pirie, S. M. Gardezi, N. C. Drucker, and J. E. Hoffman, Phys. Rev. B **101**, 121103 (2020).
[23]Y. Deng, M. Oudich, N. J. Gerard, J. Ji, M. Lu, and Y. Jing, Phys. Rev. B **102**, 180304(R) (2020).
[24]S. M. Gardezi, H. Pirie, S. Carr, W. Dorrell, and J. E. Hoffman, 2D Materials **8**, 031002 (2021).
[25]S.-Q. Wu, Z.-K. Lin, B. Jiang, X. Zhou, Z. H. Hang, B. Hou, and J.-H. Jiang, Phys. Rev. Appl. **17**, 034061 (2022).
[26]M. Rosendo López, F. Peñaranda, J. Christensen, and P. San-Jose, Phys. Rev. Lett. **125**, 214301 (2020).
[27]M. Martí-Sabaté and D. Torrent, Phys. Rev. Appl. **15**, L011001 (2021).
[28]Y. Jin, W. Wang, Z. Wen, D. Torrent, and B. Djafari-Rouhani, Extreme Mech. Lett. **39**, 100777 (2020).
[29]S. Yves, M. I. N. Rosa, Y. Guo, M. Gupta, M. Ruzzene, and A. Alù, Adv. Sci. **9**, 2200181 (2022).
[30]Y. Jin, Y. Pennec, B. Bonello, H. Honarvar, L. Dobrzynski, B. Djafari-Rouhani, and M. I. Hussein, Rep. Prog. Phys. **84**, 086502 (2021).
[31]A. V. Rozhkov, A. O. Sboychakov, A. L. Rakhmanov, and F. Nori, Phys. Rep. **648**, 1 (2016).
[32]N. N. T. Nam and M. Koshino, Phys. Rev. B **96**, 075311 (2017).
[33]E. J. Mele, Phys. Rev. B **81**, 161405 (2010).
[34]M. Oudich, G. Su, Y. Deng, W. Benalcazar, R. Huang, N. Gerard, M. Lu, P. Zhan, and Y. Jing, Phys. Rev. B **103**, 214311 (2021).